Liquid Crystals
Publication details, including instructions for authors and subscription information:
http://www.informaworld.com/smpp/title~content=t713926090

Synthesis and liquid crystalline properties of hydrazide derivatives: hydrogen bonding, molecular dipole, and smectic structures

Haitao Wang[a]; Binglian Bai[a]; Dongmei Pang[a]; Zhongfei Zou[b]; Li Xuan[b]; Fan Li[a]; Peng Zhang[a]; Lihua Liu[a]; Beihong Long[a]; Min Li[a]
[a] Key Laboratory of Automobile Materials, Ministry of Education, Institute of Materials Science and Engineering, Jilin University, Changchun 130012, People's Republic of China [b] State Key Laboratory of Applied Optics, Changchun Institute of Optics, Fine Mechanics and Physics, Chinese Academy of Science, Changchun 130033, People's Republic of China

To cite this Article Wang, Haitao , Bai, Binglian , Pang, Dongmei , Zou, Zhongfei , Xuan, Li , Li, Fan , Zhang, Peng , Liu, Lihua , Long, Beihong and Li, Min(2008) 'Synthesis and liquid crystalline properties of hydrazide derivatives: hydrogen bonding, molecular dipole, and smectic structures', Liquid Crystals, 35: 3, 333 — 338
To link to this Article: DOI: 10.1080/02678290801902556
URL: http://dx.doi.org/10.1080/02678290801902556

Liquid Crystals,
Vol. 35, No. 3, March 2008, 333–338

Taylor & Francis
Taylor & Francis Group

Synthesis and liquid crystalline properties of hydrazide derivatives: hydrogen bonding, molecular dipole, and smectic structures

Haitao Wang[a], Binglian Bai[a], Dongmei Pang[a], Zhongfei Zou[b], Li Xuan[b], Fan Li[a], Peng Zhang[a], Lihua Liu[a], Beihong Long[a] and Min Li[a]*

[a]*Key Laboratory of Automobile Materials, Ministry of Education, Institute of Materials Science and Engineering, Jilin University, Changchun 130012, People's Republic of China;* [b]*State Key Laboratory of Applied Optics, Changchun Institute of Optics, Fine Mechanics and Physics, Chinese Academy of Science, Changchun 130033, People's Republic of China*

(Received 16 May 2007; final form 8 January 2008)

A series of dissymmetric hydrazide derivatives with amino terminal group, *N*-(4-alkoxybenzoyl)-*N*′-(4′-aminobenzoyl) hydrazine (C*n*-NH_2, *n* indicates the number of carbon atoms), were designed and synthesised, and their liquid crystalline properties were investigated by means of differential scanning calorimetry, polarised optical microscopy, and wide-angle X-ray diffraction. It was found that these materials showed a SmA_d phase, and intermolecular hydrogen bonding was confirmed as the driving force. Moreover, these results were further compared with those of their parent compounds, *N*-(4-alkoxybenzoyl)-*N*′-(4′-nitrobenzoyl) hydrazine (C*n*-NO_2) and the dimers, α, ω-bis [*N*-(4-nitrobenzoyl)-*N*′-(benzoyl-4′-oxy) hydrazine] alkane (N*n*), and the effect of hydrogen bonding, dipole-dipole interactions on the smectic structures is discussed.

Keywords: hydrogen bonding; semi-bilayer structure; smectic phase; hydrazide derivatives; dipole–dipole interaction

1. Introduction

In the past few decades, much attention has been paid to hydrogen-bonded supramolecular liquid crystals (*1–3*). However, many efforts have been restricted to generating calamitic mesophases with molecules bearing a donor and/or an acceptor site at their terminals, in which hydrogen bonding along the molecular long axis is utilised to format a new and elongated mesogenic unit to stabilise the mesophase, such as the dimer of aromatic carboxyl acid (*4*) and dimerisation between the carboxyl acid and pyridyl moieties (*5–7*). Little attention has been paid to lateral intermolecular hydrogen bonding, because it is generally considered that the spinning of the rod around the long axis is suppressed by lateral hydrogen bonding, which destabilises the liquid crystal phase, while stabilising the crystal state (*8–13*).

On the contrary, we found that a very stable SmA_1 phase was generated from those dissymmetric hydrazide derivatives with terminal nitro group, *N*-(4-alkoxybenzoyl)-*N*′-(4′-nitrobenzoyl) hydrazine (C*n*-NO_2, as shown in scheme 1 a), in which lateral intermolecular hydrogen bonding was confirmed to still interact in the smectic phase, and played an important role in stabilising the mesophase (*14*). However, it was not clear why these dissymmetric hydrazide derivatives with polar terminal substituents adopted the parallel molecular packing (macroscopically should have neighbouring groups of molecules orientated in opposite directions, SmA_1), instead of the semi-bilayer SmA_d phase, as commonly found in those polar systems (*15, 16*). Further understanding of the molecular origin of this unusual behaviour could be gained by decreasing the molecular polarity, so we changed the terminal nitro group to an amino group, resulting in *N*-(4-alkoxybenzoyl)-*N*′-(4′-aminobenzoyl) hydrazine (C*n*-NH_2), as shown in scheme 1 b. Interestingly, C*n*-NH_2 exhibited a SmA_d phase. Here, we report the synthesis, liquid crystalline properties of C*n*-NH_2, and further comparison between the results of C*n*-NH_2, C*n*-NO_2, and the dimers, α, ω-bis [*N*-(4-nitrobenzoyl)-*N*′-(benzoyl-4′-oxy) hydrazine] alkane (N*n*, as shown in scheme 1 c).

2. Experimental

2.1. *Synthesis*

As shown in scheme 1, the amino derivatives (C*n*-NH_2) were prepared from their corresponding parent compounds (C*n*-NO_2) by reducing the –NO_2 group according to the literature (*17*). All the compounds were purified by repeated recrystallisation from dimethyl sulfoxide (DMSO) for further NMR, FT-IR measurements, and elemental analysis – yield >80%.

*Corresponding author. Email: minli@mail.jlu.edu.cn

ISSN 0267-8292 print/ISSN 1366-5855 online

DOI: 10.1080/02678290801902556
http://www.informaworld.com

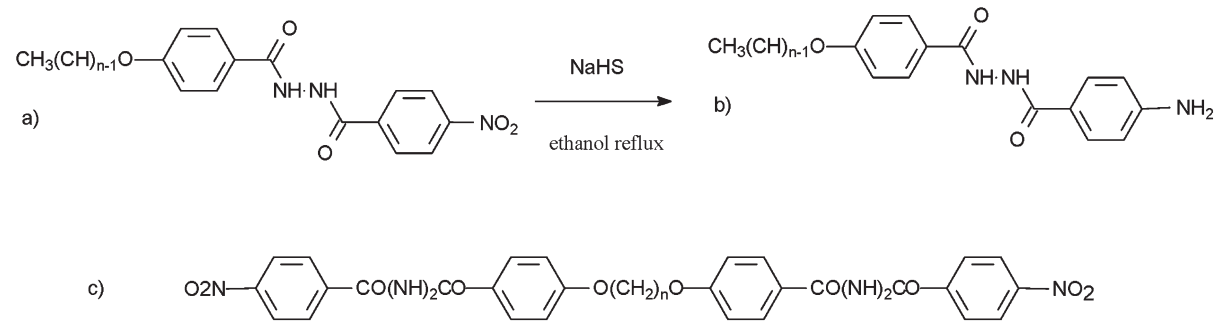

Scheme 1. Molecular structures of (a) C*n*-NO_2; (b) C*n*-NH_2(n=10, 12, 14, 16), and N*n* (n=5, 6, 10) and the synthesis of C*n*-NH_2.

2.1.1. N-(4-decyloxybenzoyl)-N′-(4′-aminobenzoyl) hydrazine (C10-NH_2).

^{1}H NMR (500 MHz, DMSO), (ppm, from tetramethylsilane (TMS)): δ=10.12 (s, 1H); δ=9.89 (s, 1H); δ=7.87 (d, 2H, J=8.7 Hz); δ=7.64 (d, 2H, J=8.5 Hz); δ=7.01 (d, 2H, J=8.8 Hz); δ=6.57 (d, 2H, J=8.5 Hz); δ=5.70 (s, 2H); δ=4.03 (t, 2H, J=6.5 Hz); δ=1.73 (m, 2H); δ=1.42 (m, 2H); δ=1.27 (m, 12H); δ=0.86 (t, 3H, J=6.8 Hz). FT-IR (KBr disc, cm^{-1}): 3404, 3321, 3259, 3231, 2953, 2922, 2853, 1630, 1606, 1594, 1560, 1519, 1448, 1433, 1415, 1396, 1309, 1285, 1253, 1181, 1171, 1118, 1097, 1050, 1015, 994, 839, 752, 722, 693, 650, 603. Anal. Calcd for $C_{24}H_{33}N_3O_3$: C, 70.04; H, 8.08; N, 10.21. Found C, 69.88; H, 8.23; N, 10.04.

2.1.2. N-(4-dodecyloxybenzoyl)-N′-(4′-aminobenzoyl) hydrazine (C12-NH_2).

^{1}H NMR (500 MHz, DMSO), (ppm, from TMS): δ=10.15 (s, 1H); δ=9.92 (s, 1H); δ=7.87 (d, 2H, J=8.2 Hz); δ=7.64 (d, 2H, J=7.9 Hz); δ=7.02 (d, 2H, J=8.3 Hz); δ=6.57 (d, 2H, J=8.0 Hz); δ=5.73 (s, 2H); δ=4.03 (t, 2H, J=6.0 Hz); δ=1.72 (m, 2H); δ=1.41 (m, 2H); δ=1.25 (m, 16H); δ=0.86 (t, 3H, J=6.6Hz). FT-IR (KBr disc, cm^{-1}): 3403, 3320, 3259, 3220, 2954, 2921, 2853, 1630, 1607, 1594, 1560, 1519, 1448, 1432, 1415, 1396, 1309, 1286, 1253, 1181, 1171, 1118, 1097, 1020, 1000, 839, 752, 722, 693, 650, 603. Anal. Calcd for $C_{26}H_{37}N_3O_3$: C, 71.04; H, 8.48; N, 9.56. Found C, 70.99; H, 8.64; N, 9.26.

2.1.3. N-(4-tetradecyloxybenzoyl)-N′-(4′-aminobenzoyl) hydrazine (C14-NH_2).

^{1}H NMR (500 MHz, DMSO), (ppm, from TMS): δ=10.13 (s, 1H); δ=9.90 (s, 1H); δ=7.87 (d, 2H, J=8.7 Hz); δ=7.64 (d, 2H, J=8.5 Hz); δ=7.01 (d, 2H, J=8.8 Hz); δ=6.57 (d, 2H, J=8.6 Hz); δ=5.70 (s, 2H); δ=4.03 (t, 2H, J=6.5 Hz); δ=1.72 (m, 2H); δ=1.41 (m, 2H); δ=1.25 (m, 20H); δ=0.85 (t, 3H, J=6.8 Hz). FT-IR (KBr disc, cm^{-1}): 3403, 3320, 3258, 3218, 2954, 2921, 2852, 1631, 1607, 1594, 1560, 1519, 1449, 1432, 1415, 1396, 1309, 1286, 1253, 1181, 1171, 1118, 1097, 1036, 1013, 1000, 840, 752, 722, 693, 650, 603. Anal. Calcd for $C_{28}H_{41}N_3O_3$: C, 71.91; H, 8.84; N, 8.99. Found C, 71.67; H, 9.03; N, 8.61.

2.1.4. N-(4-cetyloxybenzoyl)-N′-(4′-aminobenzoyl) hydrazine (C16-NH_2).

^{1}H NMR (500 MHz, DMSO), (ppm, from TMS): δ=10.17 (s, 1H); δ=9.94 (s, 1H); δ=7.87 (d, 2H, J=8.8 Hz); δ=7.64 (d, 2H, J=8.4 Hz); δ=7.02 (d, 2H, J=8.8 Hz); δ=6.57 (d, 2H, J=8.6 Hz); δ=5.75 (s, 2H); δ=4.03 (t, 2H, J=6.4 Hz); δ=1.72 (m, 2H); δ=1.41 (m, 2H); δ=1.24 (m, 24H); δ=0.85 (t, 3H, J=6.8 Hz). FT-IR (KBr disc, cm^{-1}): 3403, 3322, 3258, 3217, 2954, 2922, 2851, 1631, 1607, 1594, 1560, 1519, 1450, 1432, 1415, 1396, 1309, 1286, 1253, 1181, 1171, 1118, 1097, 1049, 1017, 1000, 840, 752, 720, 693, 650, 603. Anal. Calcd for $C_{30}H_{45}N_3O_3$: C, 72.69; H, 9.15; N, 8.48. Found C, 72.72; H, 9.34; N, 8.37.

2.2. *Characterisation*

^{1}H NMR spectra were recorded with a Bruker Avance 500 MHz spectrometer, using DMSO-*d*6 as solvent and TMS as an internal standard. FT-IR spectra were recorded with a Perkin-Elmer spectrometer (Spectrum One B). Phase transitional properties were investigated by a Mettler Star DSC 821^e, with the heating and cooling rates of 10°C/min. Texture observation was conducted on a Leica DMLP polarised optical microscope equipped with a Leitz 350 microscope heating stage. X-ray diffraction (XRD) was carried out with a Bruker Avance D8 X-ray diffractometer.

3. Results and discussion

3.1. *Hydrogen bonding*

To evaluate the effect of hydrogen bonding on the phase transitions, temperature-dependent FT-IR

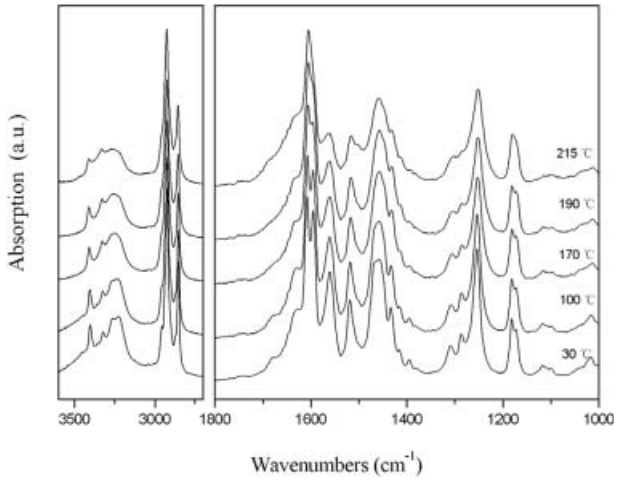

Figure 1. FT-IR spectra of C16-NH_2 at different temperatures.

spectra of C16-NH_2 have been measured (*18*). At room temperature, as shown in Figure 1, C16-NH_2 exhibits characteristic bands of N–H stretching vibrations of terminal amino group at 3403 (v_{as}), 3321 (v_s) cm^{-1} and central hydrazide group at 3258, 3213 (v) cm^{-1}, and amide I bands at 1594, 1560 cm^{-1} (strong), and 1630, 1680 cm^{-1} (weak), respectively. The observation of hydrogen bonded N-H stretching bands (3258, 3213 cm^{-1}), intense absorption of bonded C=O stretching vibrations (1594, 1560 cm^{-1}), and the small peaks of weak and non-bonded C=O stretching bands (1630, 1680 cm^{-1}) clearly indicate that the majority of the N–Hs of the central hydrazide group are associated with the C=O groups via N–H···O=C hydrogen bonding in the crystalline phase (*14, 19–20*). On heating, the N–H stretching vibration band at 3213 cm^{-1} gradually weakens, and shifts to merge with the peak at 3258 cm^{-1}, then the whole band shifts once again to higher wave numbers.

So in the smectic phase (the phase transitional temperature will be described in the following section), the $v_{N\text{-}H}$ of hydrazide groups showed a strong peak at around 3280 cm^{-1}. Simultaneously, the amide I bands at 1594, 1560 cm^{-1} became gradually weaker with ascending temperature, but after the Cr–Sm transition, they decreased dramatically and shifted to 1680 and 1630 cm^{-1}, so the later two peaks showed a sudden increase in their intensities at the Cr–Sm transition. These results strongly indicate that the hydrogen bonding became weaker during the heating process. However, the presence of the N–H stretching band at 3280 cm^{-1} and amide I bands at 1630 cm^{-1} suggest that the hydrogen bonding still interacted in the smectic phase. In addition, the N–H stretching bands (both

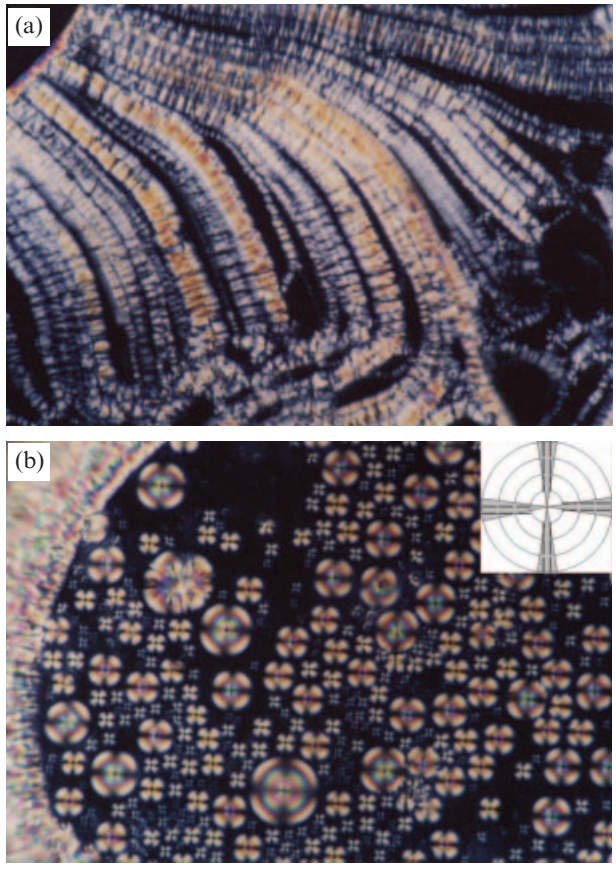

Figure 2. Textures (× 400) of: (a) C16-NH_2 at 190°C in the heating run; and (b) C10-NH_2 at 190°C in the cooling run. The inserted chart indicates that the director is normal to the smectic layers.

v_{as} and v_s) of the terminal amino group also endured a blue-shift by about 10 cm^{-1} during heating, which may imply that the N–Hs of the amino group were also hydrogen bonded, though may be much weaker than those involved in the hydrazide groups.

3.2. *Phase behaviour of Cn-NH_2*

The phase behaviour of C*n*-NH_2 was studied by polarised optical microscopy (POM) and differential scanning calorimetry (DSC). The higher homologues of C*n*-NH_2 (n=12, 14, 16) exhibit an enantiotropic SmA phase, while C10-NH_2 is monotropic. An oily streak texture with homeotropic areas was observed for the higher homologues (n=12, 14, 16) in the heating run, as shown in Figure 2 (a). While in the cooling run, only a large homeotropic area with weak birefringence was observed, which may be due to the preferred homeotropic alignment of these samples, and under the planar alignment conditions, C16-NH_2 was seen to behave optically like a uniaxial, birefringent plate of a crystal with the optic axis in the plane of the substrate, which is characteristic

Table 1. Transition temperatures and enthalpy changes of C*n*-NH_2.

Compound	Cr	*T*/°C (ΔH/kJ mol^{-1})	Meso	*T*/°C (ΔH/kJ mol^{-1})	I
C10-NH_2	•	199.5 (40.09)	•	[197.4 (2.91)]	•
C12-NH_2	•	196.5 (40.29)	•	211.7 (2.09)	•
C14-NH_2	•	192.6 (44.68)	•	215.0 (1.63)	•
C16-NH_2	•	186.8 (51.85)	•	215.2 (1.28)	•

behaviour of the SmA phase. Interestingly, a flower-like texture (as shown in Figure 2 (b)) was observed in the mesophase upon cooling from the isotropic state, which indicates that layer modulation occurred during the transition from isotropic phase to smectic phase. The extinction brushes are parallel and/or perpendicular to the polarisers, also indicating that the optical axes of molecules are normal to the smectic layers (*21*). Therefore, these mesophase can be accurately assigned to a SmA phase.

The transition temperatures and associated enthalpies are summarised in Table 1. It can be seen that the melting points descend, while the clearing points ascend as the length of the terminal chain increases, indicating that extending the length of terminal alkoxy chains increases the smectic tendencies, and stabilises the smectic phase.

3.3. *Mesophase structure*

Powder X-ray diffraction measurements have been performed on the mesophases of C*n*-NH_2. Characteristic patterns of a disordered smectic phase were observed for C*n*-NH_2, as shown in Figure 3, which contains sharp peaks in the lower-angle region, implying the formation of a layered structure, and a broad halo in the higher-angle region centred at a

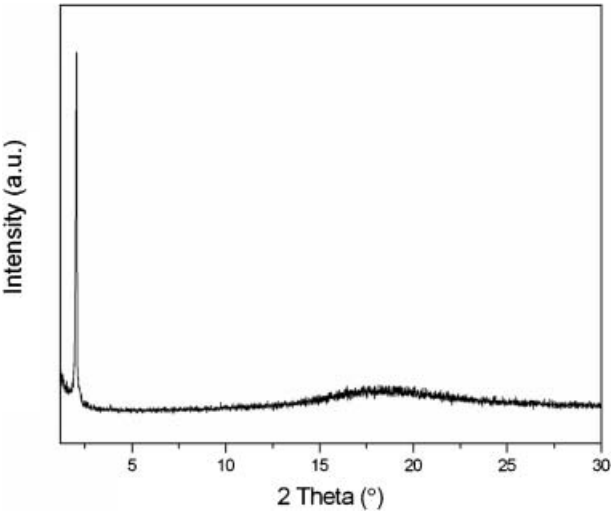

Figure 3. X-ray diffraction pattern of C16-NH_2 at 210°C.

Table 2. Summary of X-ray diffraction results of C*n*-NH_2.

Compound	Molecular length (*l*)/Å	*T*/°C	Layer spacing (*d*)/Å	*d*/*l*
C10-NH_2	28.1	190	39.3	1.40
C12-NH_2	30.6	190	42.7	1.40
C14-NH_2	33.1	180	45.1	1.36
C16-NH_2	35.6	178	47.9	1.35

spacing of 4.6 Å, indicating a liquid-like arrangement of the molecules within the layers. The layer spacing (*d*) is measured to be about 1.2–1.4 times their molecular length (*l*) (see Table 2). Considering that the director is normal to the smectic layers, as demonstrated by the textures, the partially-bilayer SmA_d phase was assigned.

Based on IR spectroscopic studies, we can reasonably defer that the intermolecular hydrogen bonding drove the semi-bilayer structure, in which the central hydrazide groups bonded to each other, and the N–Hs of the terminal amino groups may be bonded to the 'O' atoms of the alkoxy chains.

In addition, the smectic layer spacing increased dramatically on cooling, as shown in Figure 4, which may be explained by: (i) the dynamic motion of SmA phase, i.e. the molecules are arranged within the lamellae in such a way that they are often randomly tilted at slight angles with respect to the layer normal, and the tilt angle enlarged with the increasing temperature (*22*); (ii) the chain conformation, the chain extended with decreasing distortion conformations on cooling (*23–25*). However, further experiments are still required to clarify the above.

3.4. *Understanding the smectic structures*

Inspection of molecular models would highlight that there are two possible molecular arrangements to

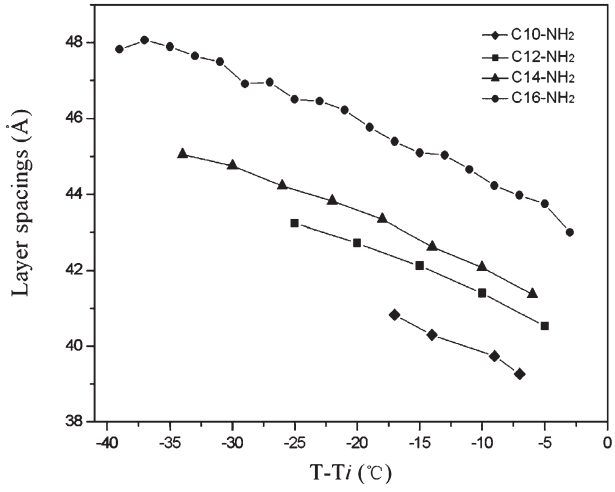

Figure 4. Temperature dependent layer spacings of C*n*-NH_2.

bring the hydrazide groups in close contact for H-bonding: the first is an anti-parallel arrangement (A configuration) with partial interdigitation; the second is a parallel head-to-head orientation (P configuration). It is interesting to compare the results of C*n*-NH_2 with that of the hydrazide derivatives terminally substituted by the nitro group (the monomers C*n*-NO_2 and dimers N*n*). By changing a nitro group into an amino group, the molecular dipole is effectively reduced, and interestingly, different phases were found in these hydrazide derivatives: these amino molecules (C*n*-NH_2) were found to form a SmA_d phase, the nitro monomers (C*n*-NO_2) were found to form SmA_1 phase (*14, 26*), while the nitro dimers (N*n*) formed the SmA_c phase (*27*). Also we noticed that the mesogenic units should take the same configuration (A configuration) in SmA_d and SmA_c phases, while in the SmA_1 phase, the molecules take the P configuration. As discussed previously, intermolecular hydrogen bonding played an important role in driving the two kinds of molecular packing.

It is still not clear why the polar molecules (C*n*-NO_2) formed the SmA_1 phase, and not the SmA_d phase. However, we can get some enlightenment from the re-entrance phenomenon observed in the polar systems, for example, a double re-entrance: N-SmA_d-N_{re}-SmA_1 (*28*). Madhusudana et al. noticed that the P configuration is more favourable than the A configuration when the intermolecular separation is below a certain value (*29*). Since it can be confirmed by FT-IR spectra that in the SmA_c phase of the dimer series (N*n*), the intermolecular separation is a little longer than that in the SmA_1 phase of the monomer system (C*n*-NO_2), for the wave numbers of stretching vibration of N–H groups in the smectic phase of the dimers (3310 cm^{-1}) is higher than that in the monomers (3290 cm^{-1}), it can be concluded that the change in the intermolecular separation induced the smectic polymorphism.

Acknowledgements

Author Dr. Haitao Wang would like to thank Professor Noel A. Clark, Dr. Edgardo Garcia, Renfan Shao, and Chenhui Zhu for their helpful discussions. The authors would like to thank the referees for their valuable comments. Also, the authors are grateful to the National Science Foundation Committee of China (Project No. 50373016), Program for New Century Excellent Talents in Universities of China Ministry of Education, Special Foundation for PhD Program in Universities of China Ministry of Education (Project No. 20050183057), and Project 985-Automotive Engineering of Jilin University for their financial support of this work.

References

(1) Kato T. *Structure Bonding* **2000**, *96*, 95–146.
(2) Paleos C.M.; Tsiourvas D. *Liq. Cryst.* **2001**, *28*, 1127–1161.
(3) Beginn U. *Prog. Polym. Sci.* **2003**, *28*, 1049–1105.
(4) Gray G.W. *Molecular Structure and the Properties of Liquid Crystals*; Academic Press: New York, 1962. p. 163, and references cited therein.
(5) Kato T.; Frechet J.M.J. *J. Am. Chem. Soc.* **1989**, *111*, 8533–8534.
(6) Gimeno N.; Ros M.B.; de la Fuente M.R. *Angew. Chem. Int. Ed.* **2004**, *43*, 5235–5238.
(7) Bai B.L.; Pang D.M.; Li M. *Chem. J. Chinese U.* **2005**, *26*, 1957–1959.
(8) Mori A.; Katahira K.; Kida K.; Takeshita H. *Chem. Lett* **1992**, *21*, 1767–1770.
(9) Mori A.; Nimura R.; Isobe M.; Takeshita H. *Chem. Lett.* **1992**, *21*, 859–862.
(10) Mori A.; Nimura R.; Takeshita H. *Chem. Lett.* **1991**, *20*, 77–80.
(11) Kajitani T.; Kohmoto S.; Yamamoto M.; Kishikawa K. *Chem. Mater.* **2004**, *16*, 2329–2331.
(12) Kajitani T.; Kohmoto S.; Yamamoto M.; Kishikawa K. *J. Mater. Chem.* **2004**, *14*, 3449–3456.
(13) Zhang D.; Zhou Q.; Ma Y.; Wang X.; Wan X.; Feng X. *Liq. Cryst.* **1997**, *23*, 357–363.
(14) Pang D.M.; Wang H.T.; Li M. *Tetrahedron.* **2005**, *61*, 6108–6114.
(15) Goodby J.W. Phase structures of calamitic liquid crystals. In *Handbook of Liquid Crystals*. Vol. 2A, Demus D., Goodby J., Gray G.W., Spiess H.W., Vill V. (Eds), Wiley-VCH: Weinheim, 1998; pp. 3–21.
(16) Gray G.W.; Goodby J.W. *Smectic Liquid Crystals, Textures and Structures*; Leonard Hill: Philadelphia, 1984; pp. 134–157.
(17) Freydank A.; Janietz S.; Schulz B. *J. Electroanal. Chem.* **1998**, *456*, 61–69.
(18) The assignments of IR absorption bands were based on the references; (a) Gunzler H.; Gremlich H. *IR spectroscopy*; Wiley-VCH, 2002. (b) Bellamy, L.J. *The Infra-red Spectra of Complex Molecules*, Vol. 1, 3rd edn, Chapman & Hall Ltd., 1975.
(19) Xue C.; Jin S.; Weng X.; Ge J.J.; Shen Z.; Shen H.; Graham M.J.; Jeong J.K.; Huang H.; Zhang D.; Guo M.; Harris F.W.; Cheng S.Z.D. *Chem. Mater.* **2004**, *16*, 1014–1025.
(20) Shen H.; Jeong J.K.; Xiong H.; Graham M.J.; Leng S.; Zheng J.X.; Huang H.; Guo M.; Harris F.W.; Cheng S.Z.D. *Soft. Matter.* **2006**, *2*, 232–242.
(21) Walba D.M. Ferroelectric liquid crystal conglomerates. In *Materials Chirality: Vol. 24 of Topics in Chemistry*; John Wiley & Sons, Inc.: New Jersey, 2003; pp. 457–518.
(22) Gray G.W.; Goodby J.W. *Smectic Liquid Crystals, Textures and Structures*; Leonard Hill: Philadelphia, 1984; pp. 1–22.
(23) Snyder R.; Maroncelli G.M.; Qi S.P.; Strauss H.L. *Science* **1981**, *214*, 188–190.
(24) Kutsumizu S.; Kato R.; Yamada M.; Yano S. *J. Phys. Chem. B* **1997**, *101*, 10666–10673.
(25) Pociecha D.; Krowczynski A.; Szydlowska J.; Gorecka E.; Glogarova M.; Przedmojski J. *J. Mater. Chem.* **1997**, *7*, 1709–1712.

(26) Wang H.T.; Pang D.M.; Xin H.; Li M.; Zhang P.; Tian W.J. *Liq. Cryst.* **2006**, *33*, 439–443.
(27) Wang H.T.; Bai B.L.; Zhang P.; Long B.H.; Tian W.J.; Li M. *Liq. Cryst.* **2006**, *33*, 445–450.
(28) Hardouin F.; Sigaud G.; Achard M.F.; Gasparoux H. *Solid State Commun.* **1979**, *30*, 265–269.
(29) Madhusudana N.V.; Rajan J. *Liq. Cryst.* **1990**, *7*, 31–40.